Impact of Seamounts on Turbulent Mixing in the Mariana Arc

Makana Paige

makmak@uw.edu

University of Washington

School of Oceanography

6/5/2026

Abstract

Internal tide production leads to increased turbulent mixing when reaching rough topography like seamounts. This leads to upwelling of abyssal waters that contain components like essential nutrients, carbon, and heat. Seamounts are common throughout the Pacific Ocean, specifically in the Western Pacific. The Mariana Arc experiences a westward dominant internal tide production with seamounts located to the west of the arc. Seamounts NW Rota – 1 and Ruby were focused on with CTD casts taken at equal depths around the seamounts. The Thorpe length scale and average dissipation rates were used to quantify turbulent mixing. Mixing was inconsistent from seamount to seamount, with a dissipation rate range approximately 2 magnitudes larger than average. Negligible differences in mixing were found between the northern and southern quadrants. Increased mixing leads to more upwelling from the Meridional Overturning Circulation (MOC). Understanding where upwelling occurs can improve our understanding of what physical influences are on the MOC.

Plain Language Summary

Internal tides are waves that move through the ocean, and they can increase mixing when they interact with features on the sea floor. This increase in mixing can lead to upwelling of important currents like the meridional overturning circulation, which is the creation and use of dense water masses. The upwelling of these currents brings essential nutrients, carbon, and heat to the surface. This study focused on the impact of seamounts on turbulent mixing and found that mixing was inconsistent between seamounts. Overall seamounts are an important feature as they are prominent throughout the Pacific Ocean and lead to increased mixing.

1. Introduction

Water at the surface in high latitudes collects information about the atmosphere's interaction with the ocean before it cools and gains salt, then sinks to join the majority of the ocean's water volume as abyssal water (De Lavergne et al., 2017). Abyssal water is an important variable in the ocean's ability to store climate relevant properties like carbon and heat (De Lavergne et al., 2017). The period of time water is isolated from the atmosphere controls the storage of these variables (Voet et al., 2015).

The interior of the ocean consists of a gradual increase in density with depth, leading to the creation of isopycnals (Finnigan et al., 2002). The thickness of the isopycnals also increases with depth, leading to the denser isopycnals having a greater area of seafloor coverage (De Lavergne et al., 2017). Within the deep-ocean, sources of density transformation are concentrated around the seafloor, leading isopycnals with large seafloor coverage to have more efficient density transformation (De Lavergne et al., 2017). This density transformation occurs through mixing of heat from the surface ocean to the deep ocean, which is required to maintain the stratification of the Bottom Boundary Layer (BBL) and lighten seawater for upwelling (De Lavergne et al., 2017). The cycle of creation and use of dense water masses is commonly referred to as the Meridional Overturning Circulation (MOC) (De Lavergne et al., 2017). The global MOC plays a vital part in the transportation and redistribution of key ocean parameters like oxygen, carbon, essential nutrients, and heat (Song et al., 2024).

Stratification of the BBL requires sufficient energy to maintain the MOC and abyssal stratification (Song et al., 2024). The energy required for deep water upwelling and BBL stratification is provided by turbulent mixing (Song et al., 2024). The main source for turbulent mixing is internal waves (Finnigan et al., 2002). Internal waves are generated when the ocean's stratification is changed which can be caused by wind and tides (Gregg et al., 2003; Voet et al., 2015). These waves propagate both horizontally and vertically throughout the ocean and can travel large distances (Gregg et al., 2003).

Barotropic (surface) and baroclinic (internal) tides interaction with rough topography produces internal tides, which are internal waves at a tidal frequency (Finnigan et al., 2002). As the internal waves propagate, they interfere with one another and turbulent mixing is produced (Finnigan et al., 2002). Rough topography experiences an increase in vertical mixing when compared to open ocean areas, alongside being an influential factor in dissipation rates, which result from the breaking of internal waves (Cusack et al., 2019; Lavelle et al., 2004; MacKinnon et al., 2013; Song et al., 2024). Submarine ridges are an example of rough topography that has efficient baroclinic tide production (Zhao & D'Asaro, 2011). Much of the tidal energy produced by ridges propagates into the ocean up to 3000 km away as baroclinic tides before dissipating as heat (Carter et al., 2006; Zhao & D'Asaro, 2011). In addition to rough topography distance from the seafloor has an impact on the magnitude of dissipation (MacKinnon et al., 2013). Vertical mixing and dissipation are contributors to upwelling of the abyssal MOC (Nakamura et al., 2021; Song et al., 2024).

Seamounts are another example of rough topography that experiences increased vertical mixing, with the primary energy coming from breaking internal waves (Holtermann et al., 2014; Song et al., 2024). As seamounts are generally isolated topographic features, water becomes accelerated around the seamount rather than flowing over as it would with a ridge (Carter et al., 2006). This leads to asymmetric mixing around the base of seamounts as an along-isobath flow, but with no enhancement of the across-isobath flow (Carter et al., 2006). Reduction of flow across the top of the seamounts makes for less effective removal of energy from barotropic tides when compared to ridges (Carter et al., 2006).

The Mariana Arc, located in the Pacific Ocean, houses both a submarine ridge and seamounts, thus it is an ideal testing ground for turbulent mixing. The arc is oriented in the North-South direction, with East-West internal tide propagation (Zhao & D’Asaro, 2011). Internal tides generated at the Mariana Arc are spatially inhomogeneous, with Saipan being a strong generation site (Zhao & D’Asaro, 2011).

With seamounts being a dominant feature of the Pacific Ocean, it is important to understand their impact on turbulent mixing and deep-water upwelling (Carter et al., 2006). This study will focus on two seamounts located in the Mariana Arc in the Northwest Pacific Ocean. The seamounts chosen are Ruby and NW Rota-1 (Figure 1). In the Mariana Arc the tidal energy flux is primarily to the west, with internal tides generated at the ridge (Zhao & D’Asaro, 2011).

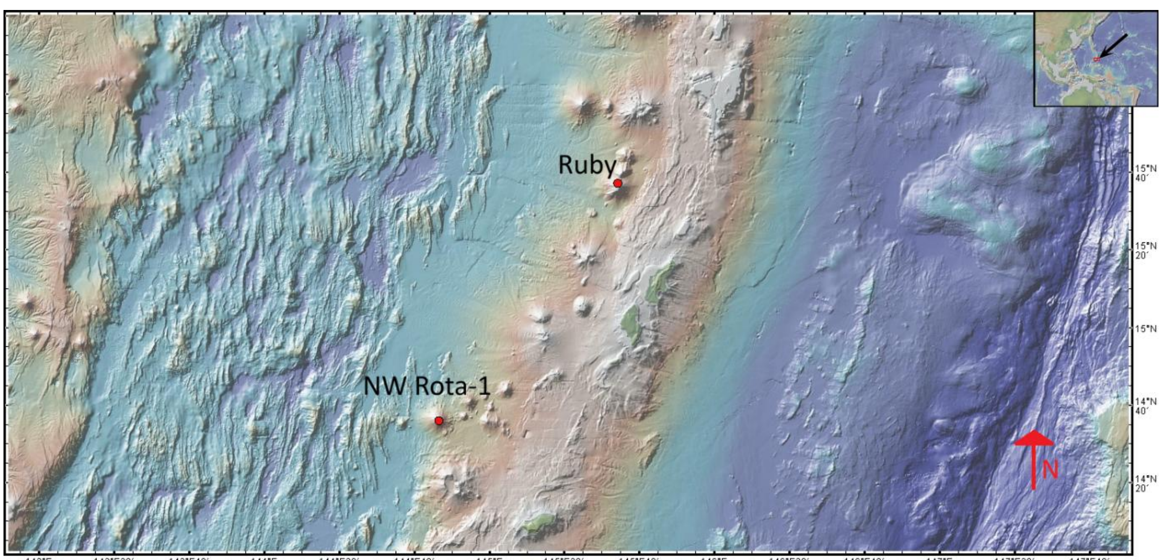

Figure 1. Topographic map of the study site, with seamounts marked.

Therefore, the objective of this study is to quantify the difference in mixing between the cardinal directions of the seamounts. The eastern quadrant of the seamounts are expected to have increased turbulent mixing compared to the western quadrant of the seamounts, with negligible difference expected between the northern and southern quadrants.

Seamounts NW-Rota 1 and Ruby are located to the west of the ridge, with the tidal energy flux hitting the eastern quadrant of the seamounts. These internal tides interact with the seamounts being a potential site for increased abyssal MOC upwelling. With the global MOC being a conveyor for essential components, it is important to understand the influences on upwelling locations.

2. Methods

2.1 Data Acquisition and Cleaning

Data used in this study was collected on the R/V *Thomas G. Thompson* on cruise TN-405 spanning from March 21- 31st 2026. Sampling occurred at two seamounts, NW Rota-1 and Ruby. The seamounts were chosen for their depths, with NW Rota-1 possessing a summit depth of 455 m and Ruby possessing a summit depth of 230 m (Table 1)(*Global Volcanism Program | NW Rota-1*, n.d.; Ruby, 2019). The summit elevations are below the surface stratification layer, which reduced the impact of surface variables like wind and waves on measurements.

Tabel 1. Latitude and longitude of Summits with summit depths

	NW Rota-1	**Ruby**
Latitude	14.601˚N	15.62˚N
Longitude	144.775˚E	144.775˚E
Summit Depth (meters)	455	230

To assess all cardinal directions of each seamount two casts were taken per quadrant. These casts were at 500 m and 1000 m below summit (Table 2), culminating in 15 CTD casts. During the cruise issues arose during sampling around Ruby, leading to one planned CTD cast being skipped. A shipboard SBE 911 plus was used for data collection.

Table 2. Station name with seamount, cardinal direction, first digit of measurement below summit depth. Latitude and longitude of casts with the water column depth and deepest CTD profile depth.

Station	Latitude	Longitude	Full Depth (m)	CTD Depth (m)
Ruby E1	15.60116	145.60083	1299	1228
Ruby E5	15.60066	145.58616	816	702
Ruby W5	15.60016	145.56066	824	700
Ruby W1	15.6	145.5475	1343	1201
Ruby N5	15.61983	145.56966	834	750
Ruby S5	15.582166	145.5755	860	801
Ruby S1	15.57167	145.57583	1393	1301
Rota E1	14.603	144.815	2114	1502
Rota E5	14.60216	144.80716	1914	1001
Rota W5	14.60266	144.76333	1076	952
Rota W1	14.6045	144.74783	1729	1601
Rota N1	14.62916	144.772333	1779	1651
Rota N5	14.617	144.77233	1227	1001
Rota S5	14.5925	144.77283	1059	1000
Rota S1	14.572	144.77283	1897	1501

Once collected CTD casts were cleaned and processed, leaving a resolution of one sample per meter. Only the downcast of profiles has been included in analysis to minimize ship and CTD/ rosette package influence, with duplicate pressures edited out after the first appearance (Gargett & Garner, 2008). The upper 300 meters was removed from analysis as it contains the mixed layer and pycnocline as the method of analysis is not appropriate for weak or strong stratification (Song et al., 2024).

2.2 Method of Analysis

Mixing was analyzed with the Thorpe scale and dissipation rates. Thorpe length scale is based on displacement, d' , which is the distance of a water parcel from its statically stable height in the water column (Cusack et al., 2019). Calculated for a given depth by

$$d' = d_f - d_i$$

here d_f represents the final depth the water parcel moved from d_i (Gargett & Garner, 2008). Overall, a positive d' value indicates downward movement of the water parcel, and a negative d' value indicates upward movement (Gargett & Garner, 2008). d' can be derived from potential density profiles calculated from measured temperature and salinity profiles (Gargett & Garner, 2008).

The Thorpe scale (L_T) is then given as the vertical distance over which the total displacements sum to zero, computed as the root-mean-square of all displacements within a complete overturn (Gargett & Garner, 2008). Calculated as

$$L_T = \overline{(d'^2)}^{1/2} \tag{1}$$

where the overbar represents an average over depth (Gargett & Garner, 2008; Song et al., 2024). In ocean environments L_T profiles calculated with density tend to have increased instances of noise within a profile compared to profiles calculated with temperature. Despite this we used L_T calculated by sorted density as temperature is not always the most influential factor for density within the ocean (Gargett & Garner, 2008). To set a minimum size for detecting overturns they cannot be thinner than twice the vertical resolution, leading to an assumption that between five and seven samples are needed to identify an overturn (Galbraith & Kelley, 1995).

The turbulent dissipation rate, used to measure strength of turbulent mixing, was used for analysis of dissipation (MacKinnon et al., 2013). Dissipation of a single overturn event is calculated from the Thorpe scale and stratification as

$$\varepsilon = a^{-2} L_T^2 N^3 \tag{2}$$

a is a constant equal to 0.8 as that is suitable for a variety of environments (MacKinnon et al., 2013; Song et al., 2024). The buoyancy frequency, N , is derived from a sorted potential density profile (Song et al., 2024). Buoyancy frequency was calculated with the equation

$$N_i = \sqrt{-\frac{g}{\rho_o}\frac{\partial\rho}{\partial z}} \tag{3}$$

where g represents gravity, ρ_o is a reference potential density, $\frac{\partial\rho}{\partial z}$ is the change in potential density over the change in depth (Park et al., 2014).

The Thorpe scale, epsilon, and buoyancy frequency were calculated in python using the Mixsea package. To quality control epsilon and buoyancy frequency a noise threshold was set to 5 x 10^{-4} with any values below being discarded.

3. Results

3.1 East – West Transect

When comparing mixing on the East - West transacts there were a variety of signals. Thorpe scales show larger overturns on the west side of the seamounts compared to the east side (Fig 2, 3). Rota stations E5 and E1 were removed from analysis as CTD casts ended greater than 600 m above the seafloor (Table 2). Only one station pair, Ruby E1 and W1, indicate larger overturns in the east (Fig 4). The Thrope displacement scale varied between stations, with those at Ruby E5 being ±5 m and those at Ruby W5 being ±20 m (Fig 2). NW Rota- 1 stations E5 and W5 share similar scale differences where E5 had a ±4 m scale and W5 had a ± 20 m scale (Fig 3). The outlier of the group with a Thorpe displacement scale of -40 m to + 20 m is Ruby E5 (Fig 4). Thorpe scales show larger overturns concentrated at the bottom of the water column (Fig 2, 3, 4).

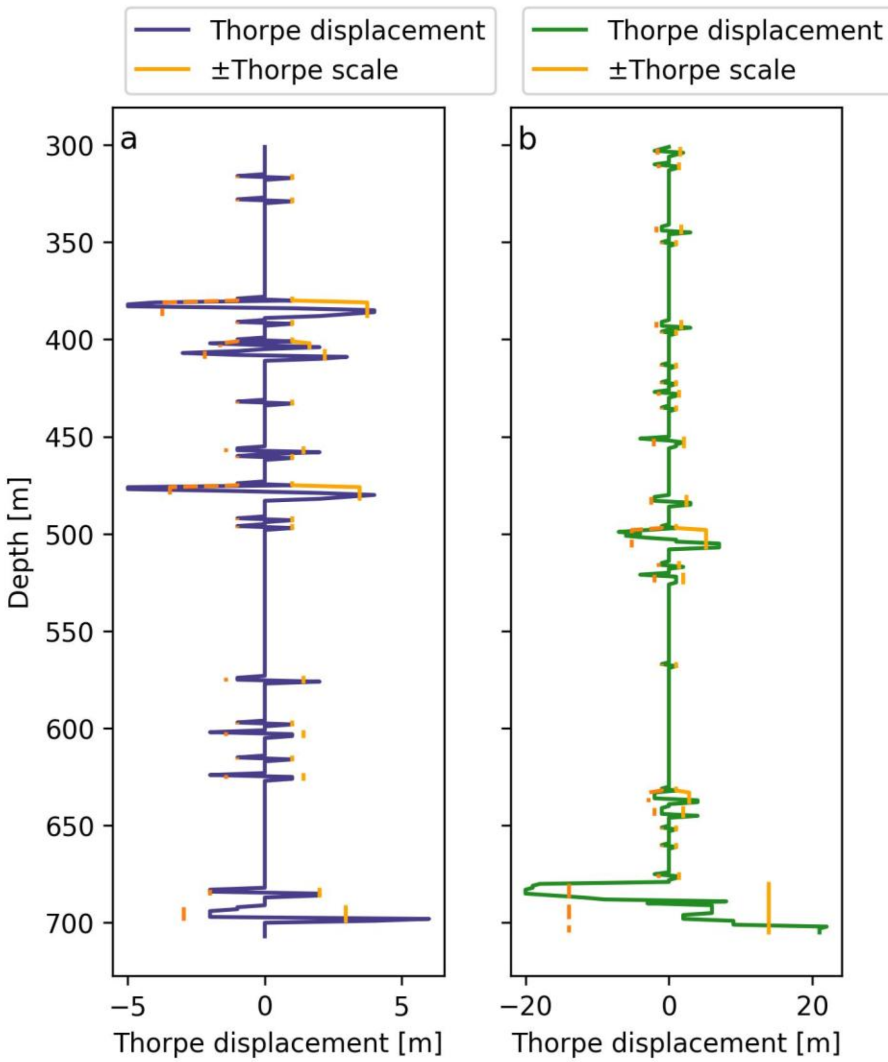

Figure 2. Profiles of Thorpe displacement and Thorpe scale (orange lines) for Ruby seamount stations (a) E5 and (b) W5.

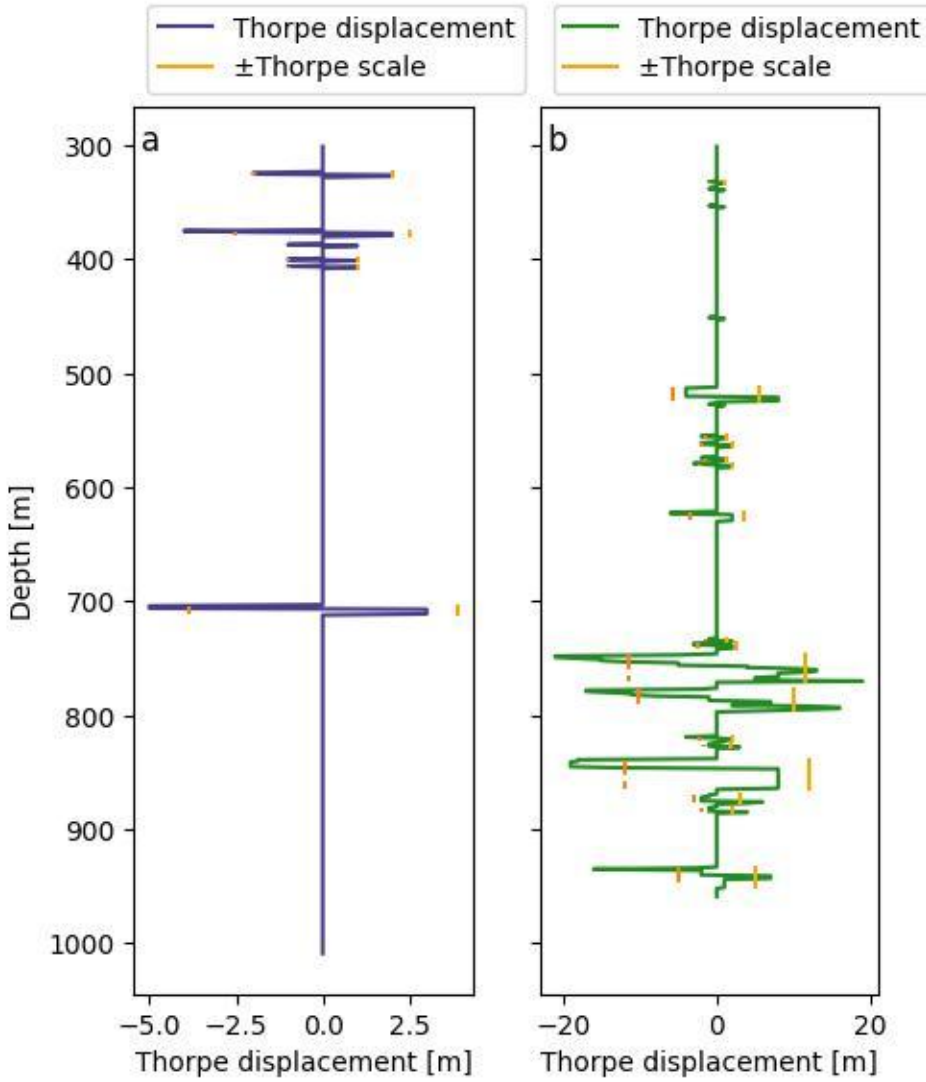

Figure 3. Profiles of Thorpe displacement and Thorpe scale (orange lines) for NW Rota-1 seamount stations (a) E5 and (b) W5.

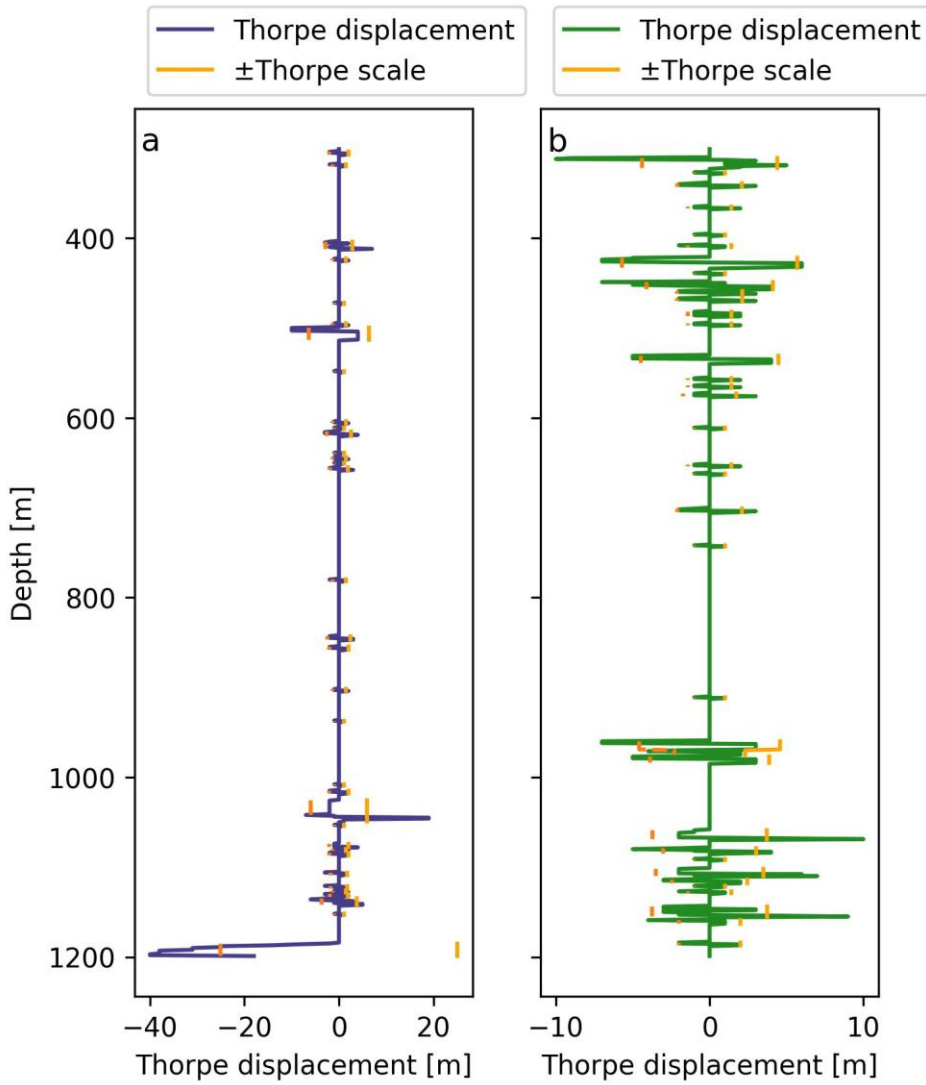

Figure 4. Profiles of Thorpe displacement and Thorpe scale (orange lines) for Ruby seamount stations (a) E1 and (b) W1.

Epsilon values, refer to equation 2, were calculated and plotted as distance from the seafloor. Both seamounts have dissipation rates concentrated between 10^{-9} and 10^{-6} W kg^{-1} on an East – West transect (Fig 5). Plotted as distance from the seafloor there is no discernible pattern within the raw epsilon values (Fig 5).

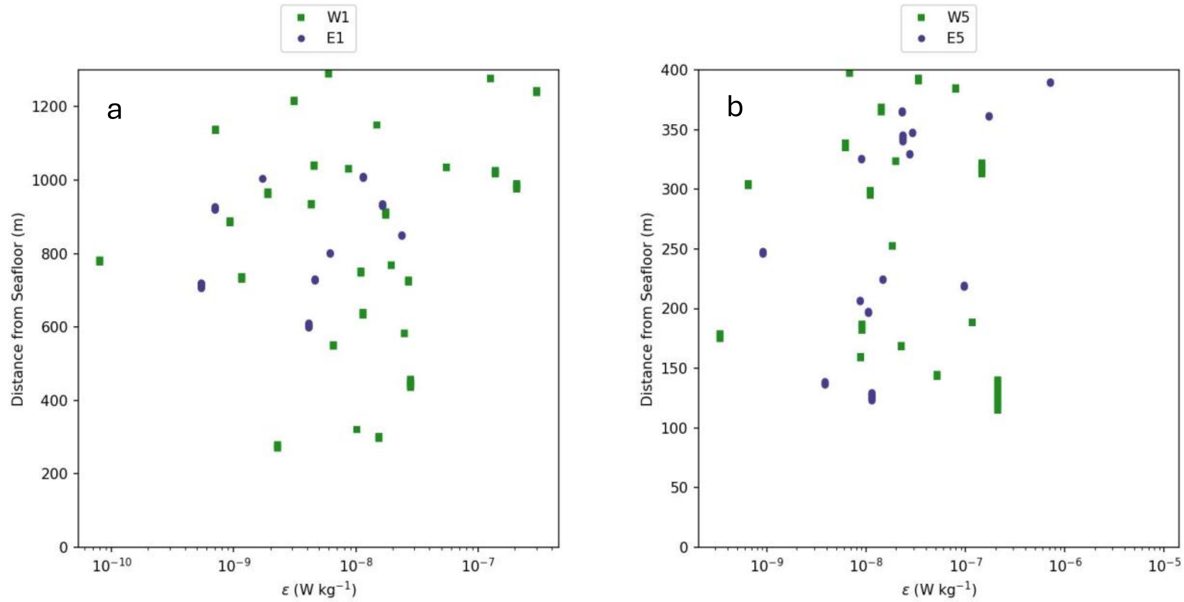

Figure 5. Calculated epsilon with all accepted values. Blue circles (green squares) are east stations (west stations). Panel a Rota stations E1 and W1, panel b Ruby stations E5 and W5.

3.2 North – South Transect

Thorpe scales on the North-South transect have smaller difference in overturn size. The maximum Thorpe displacement on the North-South transect is ±20 m, and the station pairs have very similar displacement axes (Fig 6, 7, 8). There were minimal overturns occurring at NW Rota-1 stations S1 and N1 with Thorpe displacement scales of ±4 m (Fig 6). Whereas NW Rota-1 stations N5 and S5 have similar overturn size as the East – West transect, as the Thorpe displacement scales are ±20 m (Fig 7). Concomitantly this station pair has increased mixing in the southern quadrant (Fig 7). Overall, the Thorpe scales demonstrate overturns being concentrated toward the bottom of the water column (Fig 7, 8).

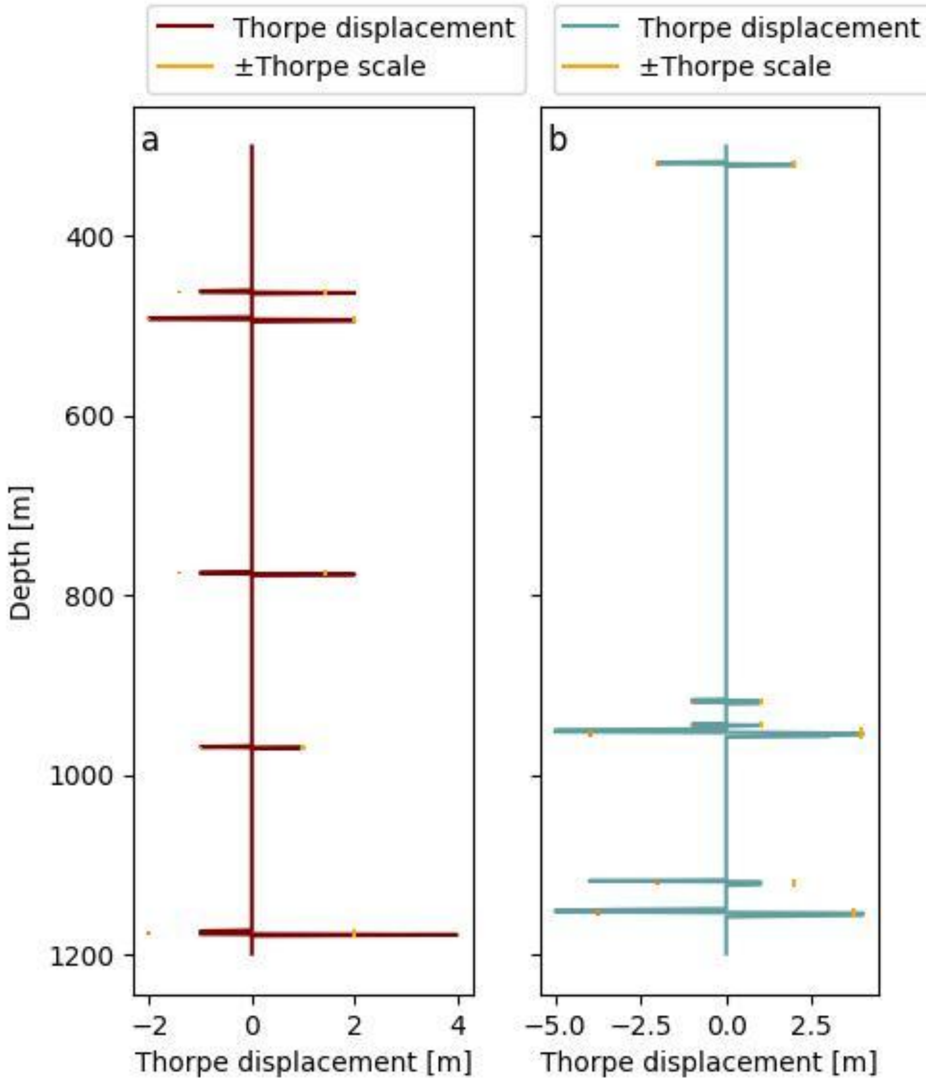

Figure 6. Profiles of Thorpe displacement and Thorpe scale (orange lines) for NW Rota-1 seamount stations (a) N1 and (b) S1.

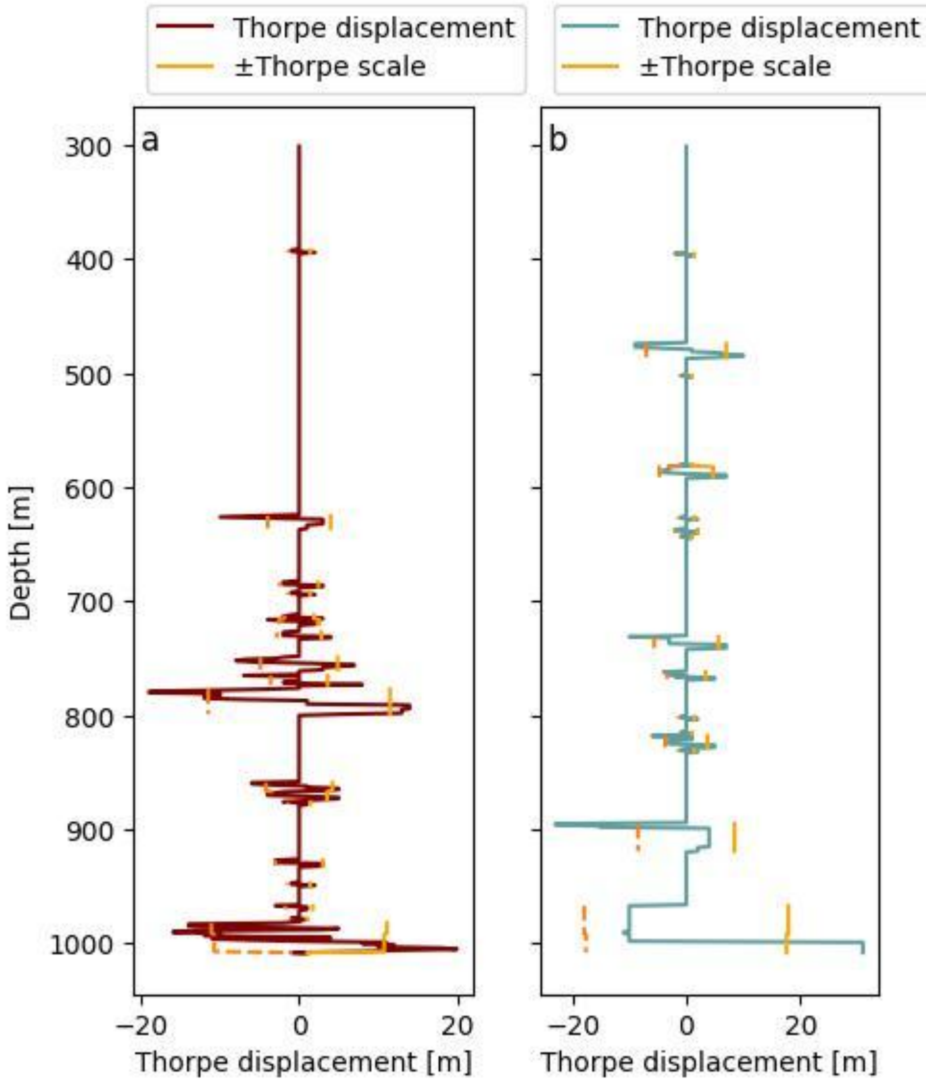

Figure 7. Profiles of Thorpe displacement and Thorpe scale (orange lines) for NW Rota-1 seamount stations (a) N5 and (b) S5.

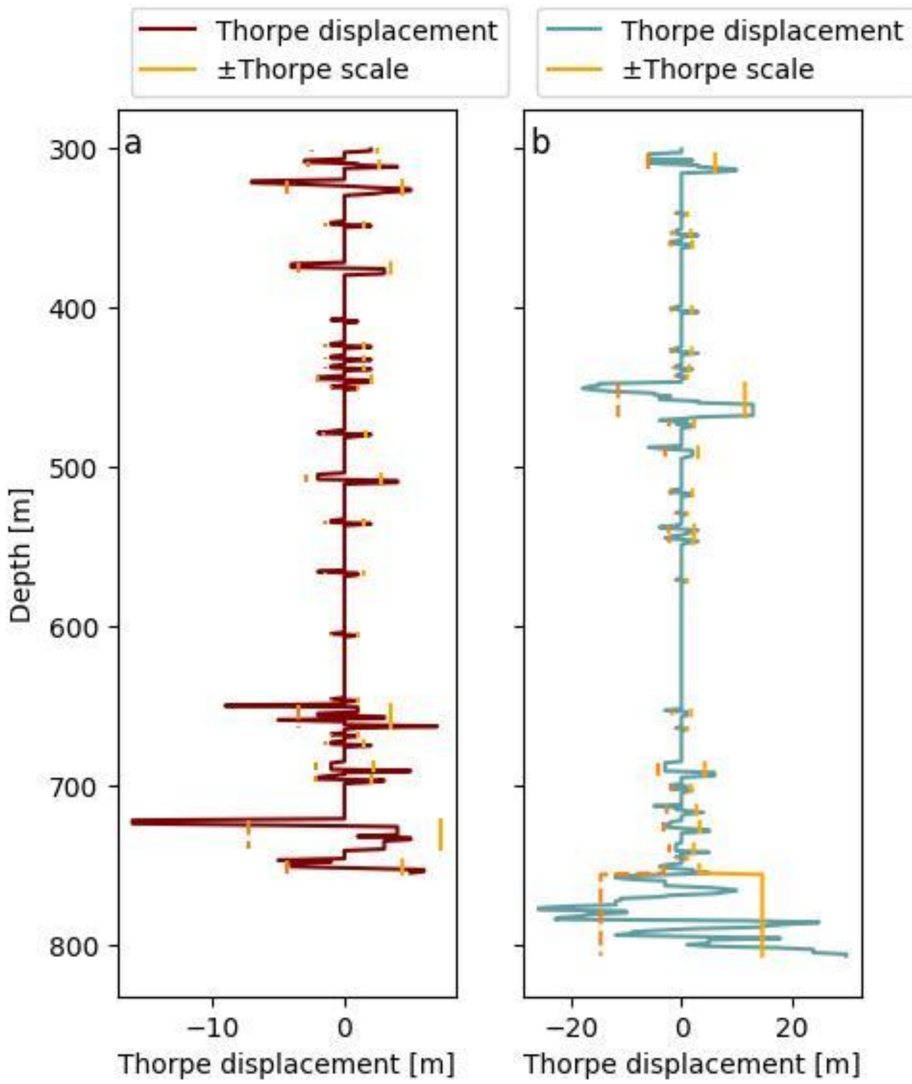

Figure 8. Profiles of Thorpe displacement and Thorpe scale (orange lines) for Ruby seamount stations (a) N5 and (b) S5.

A majority of the dissipation rates on the North – South transect are between 10^{-9} W kg^{-1} and 10^{-6} W kg^{-1}, with a maximum of 2.34 x 10^{-6} W kg^{-1}. At Ruby stations S5 and N5 the majority of epsilon was between 10^{-8} W kg^{-1} and 10^{-6} W kg^{-1} whereas at NW Rota-1 epsilon values were mostly between 10^{-9} W kg^{-1} and 10^{-7} W kg^{-1} (Fig 9).

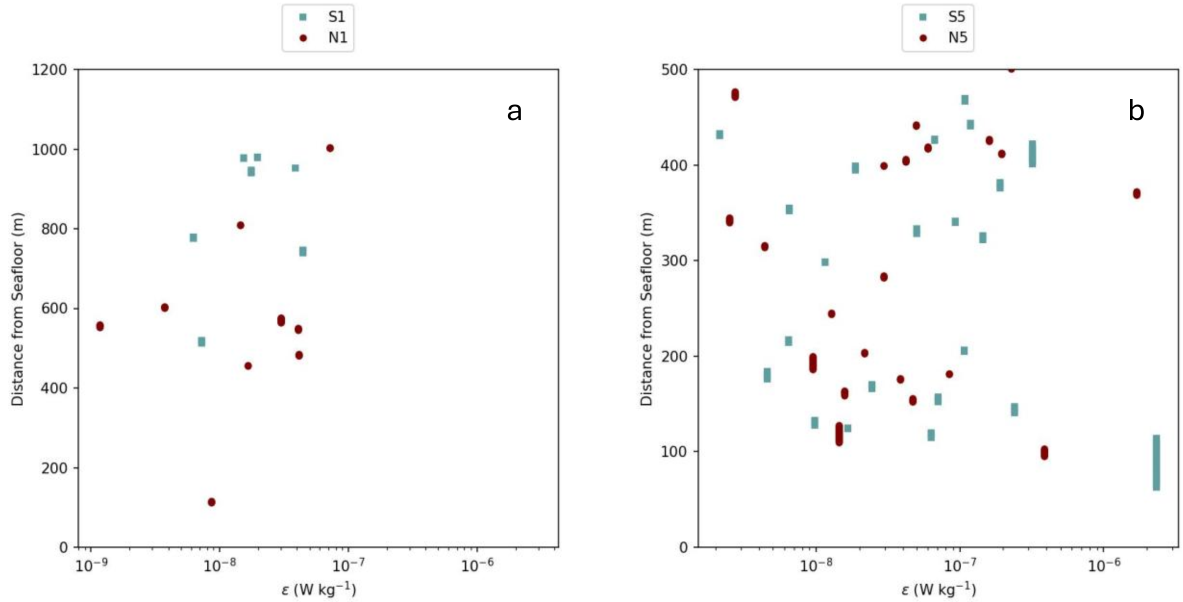

Figure 9. Calculated epsilon with all accepted values. Red circles (blue squares) are Northern (Southern) stations. Panel a NW Rota-1 stations N1 and S1, panel b Ruby stations N5 and S5.

3.3 Overall Mixing

To quantify near bottom mixing, the maximum epsilon values within 300 m of the seafloor were plotted (Fig 10, 11). At Ruby, all maximum values are within 215 m of the seafloor with the closest 87 m above the seafloor. The near bottom maximum dissipation rates range from 5.69×10^{-8} W kg^{-1} to 2.34×10^{-6} W kg^{-1} (Fig 10). NW Rota-1 maximum values are further from the seafloor ranging from 116 meters to 300 m above the seafloor. The epsilon values range from 8.65×10^{-9} W kg^{-1} to 3.54×10^{-7} W kg^{-1} (Fig 11).

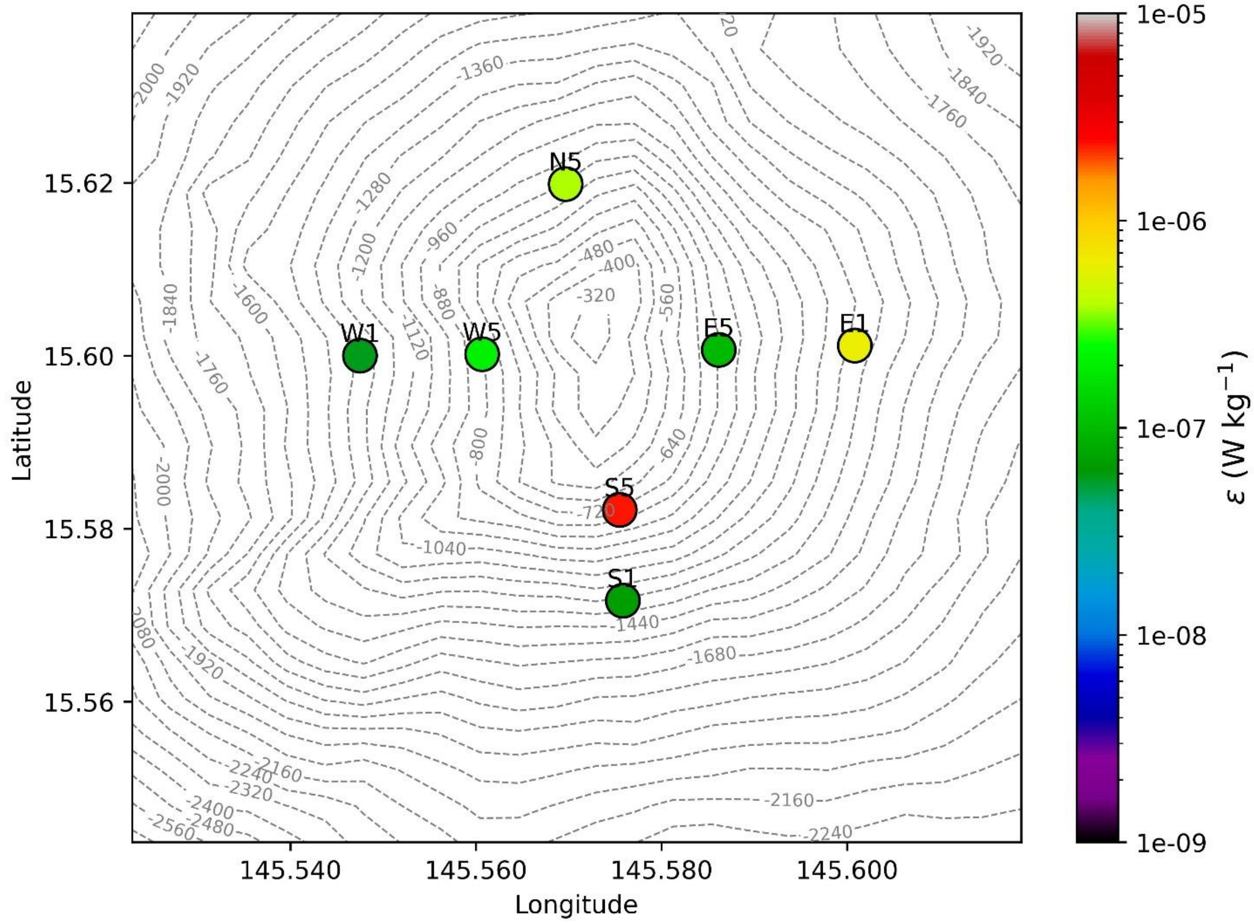

Figure 10. Maximum epsilon value within 300 meters of the seafloor at Ruby seamount. Color represents epsilon value with bathymetry in grey contours behind stations.

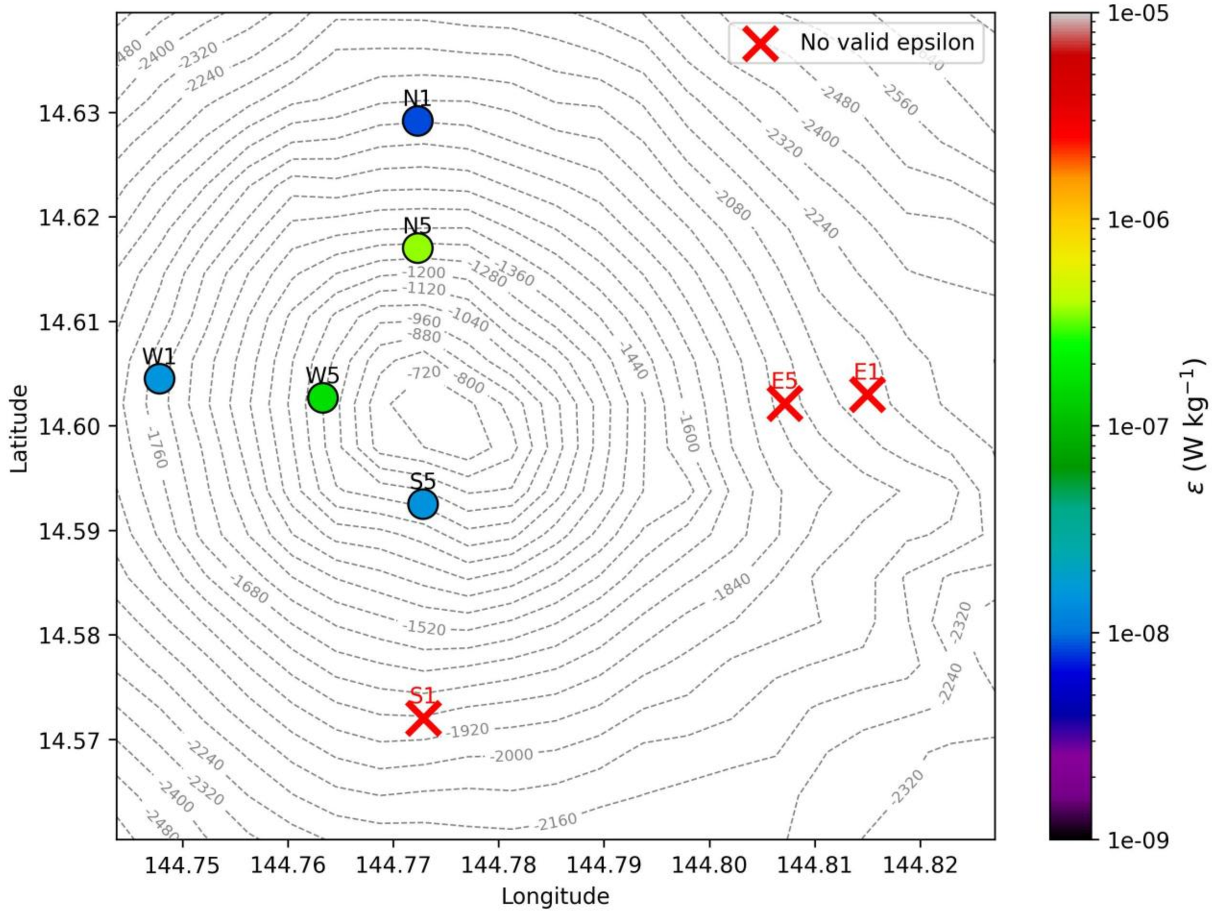

Figure 11. Maximum epsilon value within 300 meters of the bottom at Rota seamount. Color represents epsilon value with bathymetry in grey contours behind stations.

When looking at East – West transect values for Ruby the maximum epsilon at E1 is greater than at E5 whereas W5 is greater than W1 (Fig 10). On this transect E1 has the greatest epsilon value of 6.08×10^{-7} W kg^{-1} followed by W5, W1, with the smallest on the transect being E5 with a value of 9.68×10^{-8} W kg^{-1} (Fig 10). The station with the greatest epsilon value within 300 m of the seafloor is S5 with a value of 2.34×10^{-6} W kg^{-1} (Fig 10).

NW Rota-1 stations E5, E1, and S1 did not extend to within 500 m of the seafloor and contributed no valid epsilon within 300 m of the seafloor (Fig 11). Similar to Ruby, NW Rota-1 shares the pattern of W5 having a greater maximum epsilon value than W1 when looking within 300 m of the seafloor (Fig 11). The station with the greatest epsilon value was N5 with a value of 3.54 x 10^{-7} W kg^{-1} (Fig 11). Comparisons of these epsilon values between seamounts are hard to draw as three of NW Rota-1 stations E5, E1, and S1 did not extend to within 500 m of the seafloor (Fig 11).

To make comparisons, the overall maximum epsilon values were plotted as the distance from seafloor where the value occurs. Ruby has higher maximum values ranging from 2.71 x 10^{-7} W kg^{-1} to 2.34 x 10^{-6} W kg^{-1} with NW Rota-1 ranging from 4.45 x 10^{-8} W kg^{-1} to 6.92 x 10^{-7} W kg^{-1} (Fig 12 ,13).

At Ruby the quadrant with the largest dissipation rate was the Southern quadrant with values in the 10^{-6} W kg^{-1} range (Fig 12). The corresponding Northern quadrant

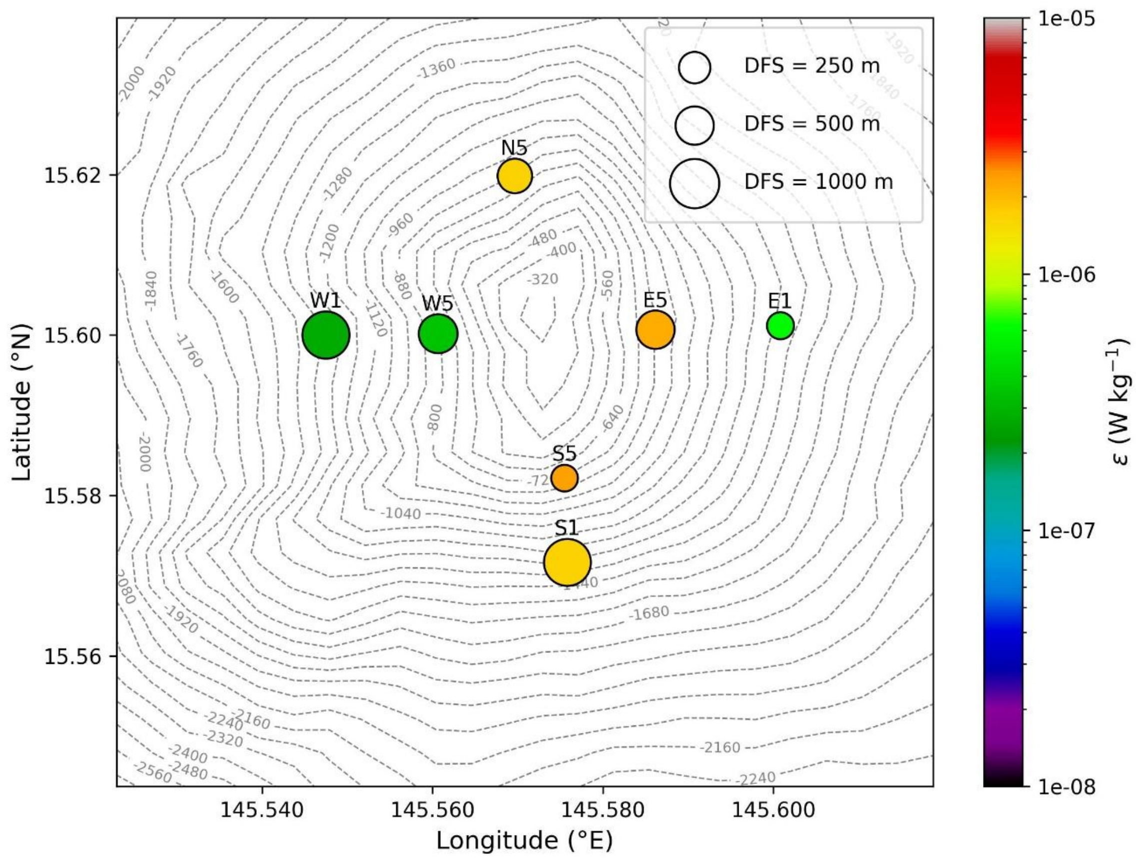

Figure 12. Ruby maximum epsilon value within the water column, color corresponds to epsilon value. The size of the circle corresponds to the depth of the value, the smaller the circle the closer to the sea floor the value is. DFS = Distance from Seafloor.

was in the same magnitude, whereas the East – West transect has an outlier value with E5 value in the 10^{-6} W kg^{-1} range compared to the 10^{-7} W kg^{-1} range of the other East and West values (Fig 12).

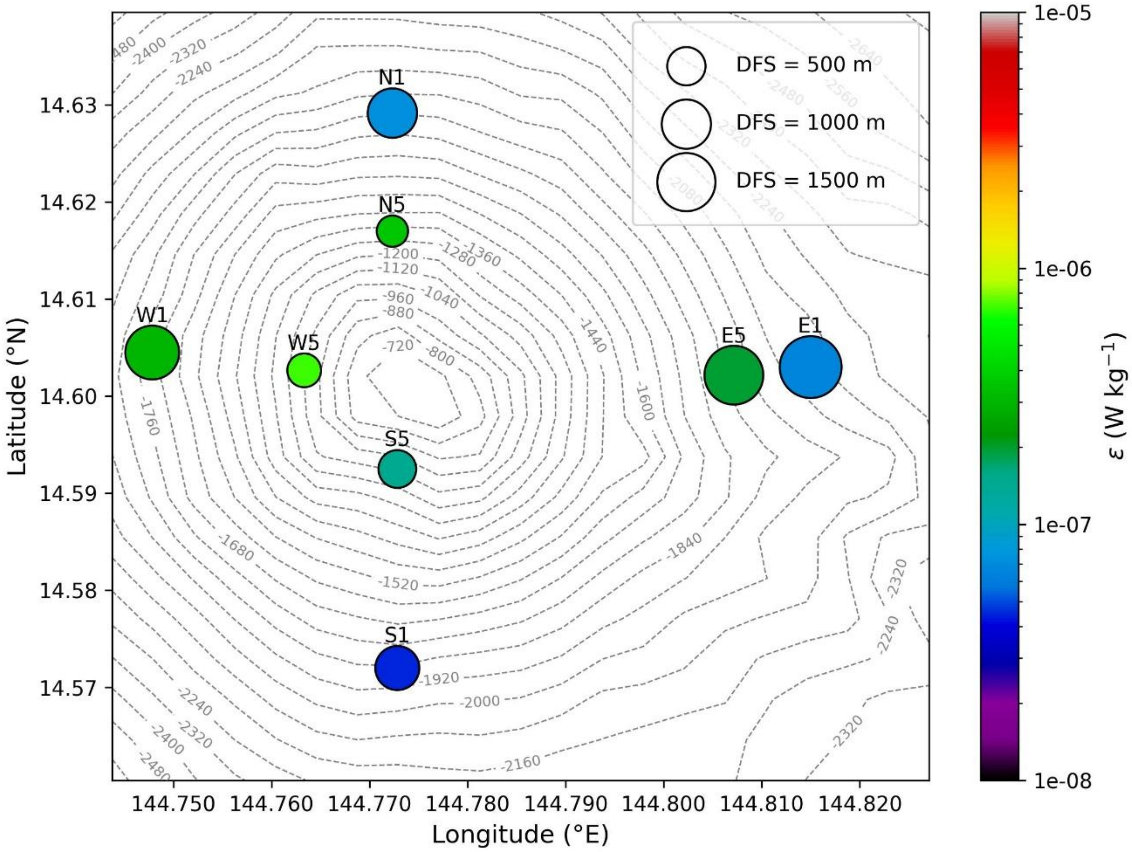

Figure 13. NW Rota-1 maximum epsilon value within the water column, color corresponds to epsilon value. The size of the circle corresponds to the depth of the value, the smaller the circle the closer to the seafloor the value is. DFS = Distance from Seafloor.

At NW Rota-1 the quadrant with the largest dissipation rate was the Western quadrant with values in the upper 10^{-7} W kg^{-1} range (Fig 13). In contrast to Ruby, the Eastern quadrant was not in the same magnitude, the values were split between the lower 10^{-7} W kg^{-1} and the upper 10^{-8} W kg^{-1} range (Fig 13).

4. Discussion

4.1 East – West Transect

Mixing on the East – West transect was inconsistent from seamount to seamount. As seamounts experience asymmetric mixing around the base, which can lead to the enhancement of mixing on a singular side the Thorpe scale was used to identify areas of large overturn (Carter et al., 2006) A pattern of the Western quadrant having larger overturns clustered at the bottom of the cast was found. The Western quadrant had Thorpe displacement scales in the ± 20 m range compared to the Eastern quadrants ± 5 m range.

To quantify the mixing that occurred the dissipation rate needs to be taken into consideration, refer to equation 2. The dissipation rate between the Eastern and Western quadrants had no discernable pattern within raw epsilon values. Comparing maximum epsilon values for the stations some patterns emerge. Ruby seamount had larger epsilon values in the Eastern quadrant for within 300 m of the seafloor and throughout the water column. When looking at the whole water column NW Rota-1 had an opposite pattern with the Western quadrant having larger epsilon values. As no measurements were taken within 300 m of the seafloor on the Eastern side of NW Rota-1, the near bottom values cannot be compared here.

Internal tides produced at the Mariana Arc propagate away from the ridge, so that the seamounts observed in this study experience westward propagating waves (Carter et al., 2006; Zhao & D’Asaro, 2011). The seamounts are oriented in a way where the quadrant that interacts with the baroclinic tide could be different for each seamount (Fig 1). Ruby is closer and further North compared to NW Rota-1, and this difference in orientation in relation to the propagating ridge could explain differences in mixing between the seamounts. Another explanation for this discrepancy in Thorpe values and dissipation rates could be a difference in the tidal cycle. As 2 - 4 hours passed between sampling the eastern quadrant versus the western quadrant at Ruby and 4 - 5 hours at NW Rota-1, the barotropic tides changed which potentially influenced mixing values.

Dissipation rates were spread out throughout the water column, with no pattern found within raw epsilon values. Dissipation within the Northwestern Pacific Ocean is typically within a range of 10^{-11} W kg^{-1} and 10^{-9} W kg^{-1} (Song et al., 2024). The range observed in this study spans 10^{-9} W kg^{-1} and 10^{-6} W kg^{-1}, two magnitudes larger than average. The increased values of the dissipation range of this study compared to the average dissipation range is inline with what is known about rough topographies impact on mixing.

4.2 North – South Transect

Little difference in Thorpe scale was observed between the station pairs of the North – South transect. A difference in mixing was observed between the S5/N5 and S1/N1 stations at NW Rota-1. When comparing S1/N1 to S5/N5 the S1/N1 stations had dramatically less overturns, with Thorpe scales of ±4 meters and S5/N5 had Thorpe scales in the ±20 m range. This Dissipation also had negligible differences. The raw epsilon values showed little trend, with the range being one magnitude smaller than the East – West transect, while still being one to two magnitudes larger than the Northwest Pacific Ocean average range. When considering the timing between the station pairs even more time passed between sampling (Ruby: 3 - 4 hours, NW Rota-1: 7 – 10 hours) than on the East – West transect.

4.3 Overall Mixing Trends

The maximum epsilon values in the Eastern quadrant at Ruby were approximately one magnitude larger than the maximum epsilon values in the Eastern quadrant at NW Rota-1. Whereas the Western quadrant maximum epsilon values were comparable between seamounts. The maximum epsilon values on the North – South transect at NW Rota-1 were more varied and further from the seafloor than at Ruby. NW Rota-1 also displays a clear pattern of maximum epsilon values increasing as they approach the summit of the seamount for the water column and within 300 m of the seafloor. Ruby displays the same pattern when looking at the maximum epsilon values within the water column, but not within 300 m of the seafloor. The increase in dissipation rate when approaching the summit aligns with seamounts increasing turbulent mixing (Song et al., 2024).

Ruby exhibits larger epsilon values than NW Rota-1, with the largest in the southern quadrant. One explanation for this is Ruby is a shallower seamount. With a summit height of 230 m it reaches into the surface stratification. Despite sample values being deeper than 300 m the shallow nature of the seamount could increase the impact of surface tides and waves. NW Rota-1 being deeper with a summit height of 445 m would have less interaction with surface stratification, reducing the impact of surface tides and waves on mixing. The difference in reach of surface stratification could lead to Ruby having increased dissipation as epsilon is based on both Thorpe scale and stratification.

When comparing the overturn size to the location of maximum epsilon values there is a difference in predicted mixing. The Thorpe scale had larger overturns in the Western quadrant with little difference appearing between the Northern and Southern quadrants. When looking at the raw epsilon values no clear pattern of West quadrant mixing appeared. The maximum epsilon values both within 300 m of the seafloor and throughout the water column did not display an increase in mixing within the Western quadrant. The difference between the overturn location and the maximum epsilon location could be explained by a difference in stratification. As previously mentioned, Ruby is shallower reaching into the surface stratification. The stratification could be impacting the dissipation rates accounting for the difference between Thorpe scale overturn location and maximum epsilon location.

One limitation of this study was the small sample size. Only visiting two seamounts gave 15 stations, which is on the smaller end for making significant connections. Another limitation of this study was the distance the final CTD casts ended compared to the seafloor depth. Many were greater than 100 m away from bottom, with the greatest distance being ~1000 m above the seafloor. This distance decreased the efficacy of the Thorpe scale method and limiting the depth range of epsilon values, which weakens the conclusions being drawn about the impact of seamounts on turbulent mixing. Further analysis with a larger sample size of seamounts would increase confidence in results.

5. Conclusion

Overall turbulent mixing is increased by rough topography, as both seamounts had dissipation rates two magnitudes larger than average for the Northwest Pacific Ocean. Seamounts are an important example of this as they are a dominant feature in the western Pacific Ocean. In this study mixing was inconsistent from seamount to seamount. Larger overturns were identified on the Western side of the seamounts as compared to the Eastern side.

Maximum dissipation rates did not correspond to the same locations where overturns occurred. At NW Rota-1 comparable dissipation occurred on the East – West transect, and

Ruby experienced higher maximum epsilon in the Eastern quadrant. In the North – South transect at NW Rota-1 there was little difference in dissipation rates between station pairs on the North – South transect, with differences found between stations within the same quadrant. Ruby had consistent maximum epsilon values on the North – South transect, with the largest epsilon value occurring in the Southern quadrant.

Following this study, more studies with increased number of seamounts and locations of seamounts with different directions of internal tides could add to an understanding of the impact of internal tides on turbulent mixing specifically at seamounts. This would add to our understanding of where upwelling occurs, as upwelling brings important nutrients and climate variables back to the surface.

6. References

Carter, G. S., Gregg, M. C., & Merrifield, M. A. (2006). *Flow and Mixing around a Small Seamount on Kaena Ridge, Hawaii*.

Cusack, J. M., Voet, G., Alford, M. H., Girton, J. B., Carter, G. S., Pratt, L. J., Tan, S., & Pearson-Potts, K. A. (2019). Persistent turbulence in the samoan passage. *Journal of Physical Oceanography*, *49*(10), 3179–3197. https://doi.org/10.1175/JPO-D-19-0116.1

De Lavergne, C., Madec, G., Roquet, F., Holmes, R. M., & McDougall, T. J. (2017). Abyssal ocean overturning shaped by seafloor distribution. *Nature*, *551*(7679), 181–186. https://doi.org/10.1038/nature24472

Finnigan, T. D., Luther, D. S., & Lukas, R. (2002). Observations of Enhanced Diapycnal Mixing near the Hawaiian Ridge. *Journal of Physical Oceanography*.

Galbraith, P. S., & Kelley, D. E. (1995). Identifying Overturns in CTD Profiles. *Journal of Atmospheric and Oceanic Technology*, *13*, 688–702.

Gargett, A., & Garner, T. (2008). Determining Thorpe scales from ship-lowered CTD density profiles. *Journal of Atmospheric and Oceanic Technology*, *25*(9), 1657–1670. https://doi.org/10.1175/2008JTECHO541.1

Global Volcanism Program | NW Rota-1. (n.d.). Smithsonian Institution | Global Volcanism Program. https://volcano.si.edu/volcano.cfm?vn=284211

Gregg, M. C., Sanford, T. B., & Winkel, D. P. (2003). Reduced mixing from the breaking of internal waves in equatorial waters. *Nature*, *422*(6931), 513–515. https://doi.org/10.1038/nature01507

Holtermann, P. L., Burchard, H., Gräwe, U., Klingbeil, K., & Umlauf, L. (2014). Deep-water dynamics and boundary mixing in a nontidal stratified basin: A modeling study of the Baltic Sea. *Journal of Geophysical Research: Oceans*, *119*(2), 1465–1487. https://doi.org/10.1002/2013JC009483

Lavelle, J. W., Lozovatsky, I. D., & Smith IV, D. C. (2004). Tidally induced turbulent mixing at Irving Seamount - Modeling and measurements. *Geophysical Research Letters*, *31*(10). https://doi.org/10.1029/2004GL019706

MacKinnon, J., St Laurent, L., & Naveira Garabato, A. (2013). *3.3: Diapycnal mixing processes in the ocean interior*.

Nakamura, H., Inoue, R., Nishina, A., & Nakano, T. (2021). Seasonal variations in salinity of the North Pacific Intermediate Water and vertical mixing intensity over the Okinawa Trough. *Journal of Oceanography*, *77*(2), 199–213. https://doi.org/10.1007/s10872-020-00585-z

Park, Y. H., Durand, I., Lee, J. H., & Provost, C. (2024). Revisiting Thorpe scale analysis and diapycnal diffusivities in Drake Passage. *Frontiers in Marine Science*, *11*. https://doi.org/10.3389/fmars.2024.1444468

Park, Y. H., Lee, J. H., Durand, I., & Hong, C. S. (2014). Validation of Thorpe-scale-derived vertical diffusivities against microstructure measurements in the Kerguelen region. *Biogeosciences*, *11*(23), 6927–6937. https://doi.org/10.5194/bg-11-6927-2014

Ruby. (2019, July 19). USGS. https://www.usgs.gov/volcanoes/ruby

Song, Q., Zhou, C., Xiao, X., Xun, H., Tian, Z., Yang, Q., Zhao, W., & Tian, J. (2024). Spatial and Temporal Variability of Turbulent Mixing in the Deep Northwestern Pacific. *Journal of Geophysical Research: Oceans*, *129*(7). https://doi.org/10.1029/2023JC020864

Thorpe Scales — mixsea 0.2.0 documentation. (2021). Readthedocs.io. https://mixsea.readthedocs.io/en/v0.2.0/thorpe_scales.html

Voet, G., Girton, J. B., Alford, M. H., Carter, G. S., Klymak, J. M., & Mickett, J. B. (2015). Pathways, volume transport, and mixing of abyssal water in the Samoan Passage. *Journal of Physical Oceanography*, *45*(2), 562–588. https://doi.org/10.1175/JPO-D-14-0096.1

Zhao, Z., & D’Asaro, E. (2011). A perfect focus of the internal tide from the Mariana Arc. *Geophysical Research Letters*, *38*(14). https://doi.org/10.1029/2011GL047909